# *B6-P1* FATIGUE DAMAGE IN A FIBRE REINFORCED ALLOY

J. L. Rossi, R. Pilkington and R. L. Trumper*
*Materials Science Centre, University of Manchester/UMIST, Grosvenor St., Manchester M1 7HS, UK*
**A.R.E. Holton Heath, Poole, Dorset BH16 6JU, UK*

**Abstract**

The fatigue damage behaviour of two batches of composite material produced by a liquid metal infiltration technique was examined by uniaxial tension-tension fatigue tests. The material consisted of a cast aluminium alloy reinforced with a continuous boron fibre coated with silicon carbide. The fatigue tests suggested that the composite life was only slightly sensitive to repeated tensile loading at 0°and 10°fibre orientation. It was shown that the mechanism by which the composite damage occurred depended on fibre and second phase breakage which led to transverse matrix cracks. Dislocation density measurements, on either tensile or fatigue tested specimens, revealed no general change when compared to the as- received material. However, the presence of prismatic loops and dislocation debris in the fatigued material was observed. A comparison between a damage model developed for diffusion bonded material and some experimental results suggested that matrix fatigue damage could be avoided , provided that the stresses were below a given value. Conversely however, the allowable matrix stresses could not be predicted from an examination of the matrix material in isolation.

## 1. Introduction

Several authors [1-5] have shown that changes in stiffness are indicative of tensile fatigue damage in composite laminates. In metal matrix composites several papers have been published on the boron/aluminium system, usually manufactured by diffusion bonding [1,2,3,4,6]. Interest in the liquid metal infiltration technique is recent because early developments were restricted by quality of fibre supply and adverse interfacial reactions [7].

Previous work [1, 4] based on diffusion bonded material has shown that boron/aluminium laminates can develop significant matrix cracking when fatigued. However, the fatigue damage may be contained, if the cyclic load amplitude is limited and does not cause stress levels in the matrix to exceed the endurance limit for a given number of cycles.

It is known that materials subjected to variable repeated loads in the plastic range can fail by cyclic plastic straining, or alternatively can shake down, i.e. resume an elastic deformation mode after some plastic strain cycles [8,9].

A simple mechanical model analysis of fatigue behaviour in metal matrix composites has been described by Dvorak and Tarn [1]. The determination of shake down stress range is done by a two parameter isostrain model. If $\sigma_y^m$ denotes the magnitude of the uniaxial flow stress of the matrix material in the annealed condition, then the proportional limit of an initially stress free composite is;

$$S_y = \sigma_y^m E_o/E_m \qquad (1)$$

where $E_o$ and $E_m$ are the composite and matrix modulus of elasticity, respectively.

It has also been shown that a prediction of fatigue limit is possible if the following equation defines the shake down stress range of the composite;

$$S_{max} - S_{min} \leq 2S_y \qquad (2)$$

Later, the work of Dvorak and Johnson [3] has shown that the onset of internal damage appears to coincide with the shake down range. This fatigue behaviour analysis led to the development of a damage model for laminates [4], where the bounds on the matrix stress range were modified. An analysis was developed to predict the decrease in laminate secant modulus caused by matrix damage. In this model the matrix starts cycling plastically. As cracks develop due to plastic cycling, the effective modulus is reduced for the portion of the matrix cycle that is in tension. The model presents simple equations to approximate the effective matrix modulus due to cracking at an assumed cyclic strain behaviour. It also proposes that if the stress range is kept below a certain minimum value, there will be no significant accumulation of fatigue damage. For a stress range greater than this value, there is a damage accumulation region where stiffness loss is observed.

## 2. Experimental

*2.1 Composite*

The composite material used in this work was manufactured by a liquid metal infiltration technique. It was produced [10] by cutting suitable lengths of the fibre tape that were then laid in a split metal die. Once the fibres were in position, the die was closed and preheated. After this, the die and the molten metal reservoir chamber were evacuated. When all parameters had been fulfilled, the melt chamber was pressurized and the liquid metal was forced into the die infiltrating the fibres.

The matrix used to infiltrate the fibres was an aluminium alloy of excellent castability designated L99 and had a composition similar to the ASM A356.0 [11]. The chemical compositions are listed in Table 1. The fibres were boron, of diameter 0.142 mm, with a 2μm thick silicon carbide coating. The SiC coating protects the boron from reacting with aluminium at elevated temperatures [12].

*2.2 Mechanical testing*

Two series of composite material were supplied, one with an average volumetric fraction of fibres around 28% and the other with around 48%. From these materials, specimens were cut with fibre orientation at 0°, 10° and 90° using a diamond wheel to minimize surface damage due to the cutting operation. The specimens at 0° and 10° were cut as rectangular coupons 75 mm long and 8 mm wide, at the end of which aluminium tapered tabs were epoxy -bonded for gripping purposes. For the 90° specimens the width was 20 mm and the length depended on slab geometry.

Before any mechanical testing, the specimens were radiographed to detect major defects and fibre agglomeration. This fibre agglomeration is caused by the metal liquid front passing through the fibres causing fibre misalignment and volumetric fraction changes.

The material in the as received condition was tensile and fatigue tested using a closed-loop servo-hydraulic machine. The fatigue tests were performed in tension-tension mode at 20 Hz, except when the stress-strain data were taken, since equipment used to take the stress-strain data only allowed measurements to be performed at very low frequencies, e.g. 0.02 H7J.

The strain was measured by two strain gauges wired in series (grid size: 6.35 mm × 3 mm) and located on both sides of the specimens. The experimental apparatus was designed to fit two additional dummy strain gauges located next to the specimen. This circuit combination eliminated bending and thermal strains that may affect the effective strain measurement.

All the specimens were cycled at a constant stress level. except a number unloading to zero stress followed by subsequent reloading to the previous stress level. The stress-strain data were taken at intervals to record the modulus change as function of number of cycles. To evaluate the amount of fatigue damage inferred from the changes in elastic modulus, it is necessary to decide how this modulus variation is measured and how it is normalized.

During specimen loading, the stress-strain behaviour follows path OAB in Fig. 1 and it is characterised by an initial linear region, path OA, followed by a non-linear region path AB. The linear region corresponds to the region of truly elastic behaviour of both matrix and fibre [13], this elastic modulus will be referred here as the initial loading modulus $E_0$. Straining the composite in the non linear region and relaxing the applied stress, the stress-strain behaviour of the composite follows path BCD, this unloading is characterized by a linear portion followed by a non-linear portion. From the linear portion is possible to measure the unloading modulus $E_{un}$. If series of load-unload cycles are repeated, path EF, stress-strain loops are developed and depending on the stress range, they can be open with permanent set, open without any permanent strain or completely closed. From the open loops is possible to measure the unloading modulus $E_{un}$ and the secant modulus $E_S$.

The fatigue damage can be evaluated by plotting the fractional change of elastic modulus versus number of cycles. The fractional change of elastic modulus $\Delta E$ is defined as follows:

$$\Delta E_s = \frac{E_s - E_{s2}}{E_{s2}} \qquad (3)$$

where $\Delta E_S$ is the fractional change of secant modulus, $E_S$ is the secant modulus at certain number of elapsed fatigue cycles, and $E_{S2}$ is the secant modulus at the second cycle (Fig. 1).

The mechanical properties of the matrix prior to infiltration were also both tensile and fatigue evaluated. Some fibres, with a gage length of 50 mm, were also tensile tested before infiltration.

*2.3 Metallographic examination*

Specimens for metallographic examination were ground using SiC paper down to grit 4000, prepolished in 0.25 μm diamond paste and finally polished in colloidal silica suspension.

The specimens for observation in the transmission electron microscope (TEM) were prepared by electrical

discharge trepanning discs either on the transverse or the longitudinal sections. After mechanically polishing these discs to thickness of about 300 μm, they were dimpled to a centre thickness of about 30 μm and further ion thinned till perforation.

Fractured specimens were examined in the scanning electron microscope (SEM) either on the fracture surface or in polished longitudinal sections to detect where cracks nucleate and to determine the fracture mode.

## 3. Results and Discussion

### *3.1 Microstructural characterization*

#### *3.1.1 28% fibre volume fraction series*

The matrix used to infiltrate the fibre is an aluminium alloy containing primarily Si and Mg. During the infiltration process, the molten aluminium alloy loses Mg and picks up other elements from the apparatus used. This modifies the original alloy composition by increasing the number and level of impurities like Ni, V and mainly Fe and Cr.

The microstructure in the longitudinal direction of the composite, i.e. parallel to the fibre direction, shows that the dendritic structure is not well defined (Fig. 2). There is precipitation during the solidification of thin platelets identified as FeSiAl interspersed with Si needles or rods. The microstructure also shows a precipitation of a globular phase next to the fibres identified as FeSiCrAl. According to the literature [14,15], different and complex intermetallic phases containing Al, Fe and Si are formed in aluminium alloys depending on the local segregation. Most of these phases have large unit cells with complex crystal structures. A bcc FeSiAl phase is probably not all equilibrium phase but is thought to be stabilized by the presence of transition elements such as Mg or Cr that can dissolve in its structure [14,16].

Transmission electron microscopy shows that the interfaces between the SiC coating and the aluminium alloy matrix consist of four main types as follow. The first type can be described as a product of contact between the SiC and the aluminium alloy. This interface is prone to reaction producing aluminium carbide that grows from the SiC into the aluminium (Fig.3). The second type of interface consists of SiC and the free Si as twinned flakes (Fig.4). The third type of interface occurs between the SiC and the intermetallics. The fourth type of interface can be described as an amorphous layer, in which selected area diffraction patterns always give very diffuse rings. Energy dispersive chemical analysis in this area reveals the presence of Al, Si, Fe, Na. Mg, P, S, Cl, P and Ca. This layer could be slag segregation entrapped between fibres or any burnt surface contaminating agent (Fig.5). TEM also has shown that the dislocation density in the aluminium alloy matrix, away from any second phase particle or fibre, is high, $\sim 3.5 \times 10^{13}$ m$^{-2}$, Fig.6. One reason for this high dislocation density may be deformation due to the difference in thermal expansion coefficient (~5:1), but there is the additional complication that the ion thinning process may introduce dislocations [17].

#### *3.1.2 48% fibre volume fraction series*

The microstructure in the longitudinal direction shows the primary aluminium and the eutectic Al - FeSiAl - Si, but the FeSiCrAl globular phase has not been observed. In this case the dendritic structure is well defined and clearly the last part to be solidified occurs at the fibre surface since the eutectic is surrounding and in contact with the fibres (Fig.7). TEM dislocation density measurement shows a slight inferior value, $\sim 3.0 \times 10^{13}$ m$^{-2}$, than the 28% fibre volume fraction material. It should be mentioned that the standard TEM dislocation density measurement usually involves many uncertainties like actual foil thickness, mechanical or ion thinning damage, that could nullify attempts to determine the effect of different volume fraction on the dislocation density. According to the literature, the average dislocation density for different composite material in the as manufactured or annealing condition is high and around $10^{14}$ m$^{-2}$. For example the work of Arsenault and Fisher [18] on an aluminium alloy reinforced with a 20% β-SiC fibre in the annealed condition shows a dislocation density of $2 \times 10^{14}$ m$^{-2}$. The investigation of Hancock and Grosskreutz [19] on an aluminium alloy reinforced with 25% stainless-steel wires in the as quenched condition reports a dislocation density around $10^{14}$ m$^{-2}$. It is worth mentioning that the TEM specimens from this last work were prepared by jet polishing and this could rule out a major effect of the ion thinning process.

### *3.2 Tensile properties*

The tensile properties were measured for the series 28% and 48% fibre volume fraction at fibre orientations of 0°, 10° and 90°. The tensile properties were also evaluated for the matrix material prior to infiltration and on the bare fibres as well. Table 2 shows the tensile tests results with the confidence interval of 95% assuming a normal distribution, except for the fibres. For the 28% series, it was possible to evaluate the matrix properties in the actual casting conditions. In some strips, a movement of the fibre preform had occurred inside the die during the infiltration manufacture, thus leaving a portion of the strip without fibres. This matrix portion was appropriately sectioned and tensile tested. This fact had allowed a comparison of tensile properties of the matrix in different

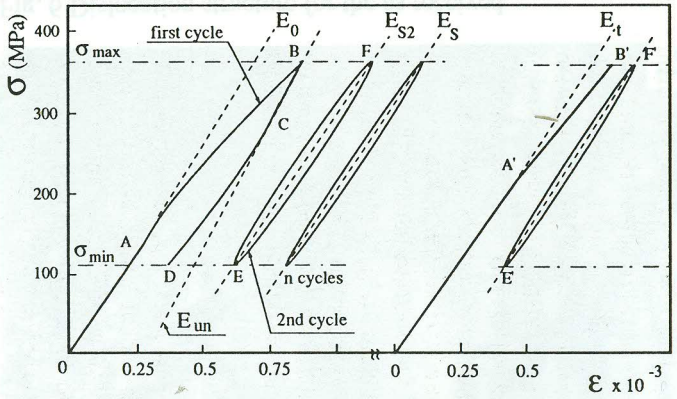


Fig. 1 Typical experimental stress-strain curves as a function of number of cycles for the 28% series material at 0° orientation.

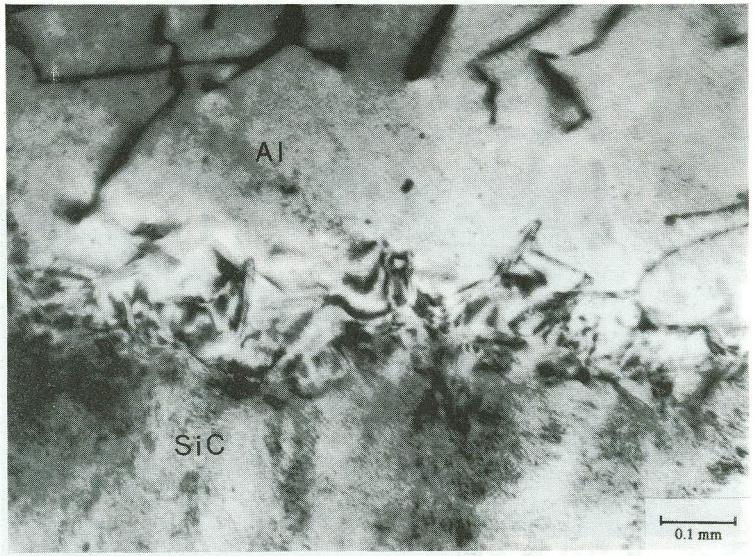


Fig. 3 Transmission electron micrograph of the aluminium alloy and SiC coating interface. This picture shows that a reaction between the aluminium and the SiC has occurred during the infiltration process.

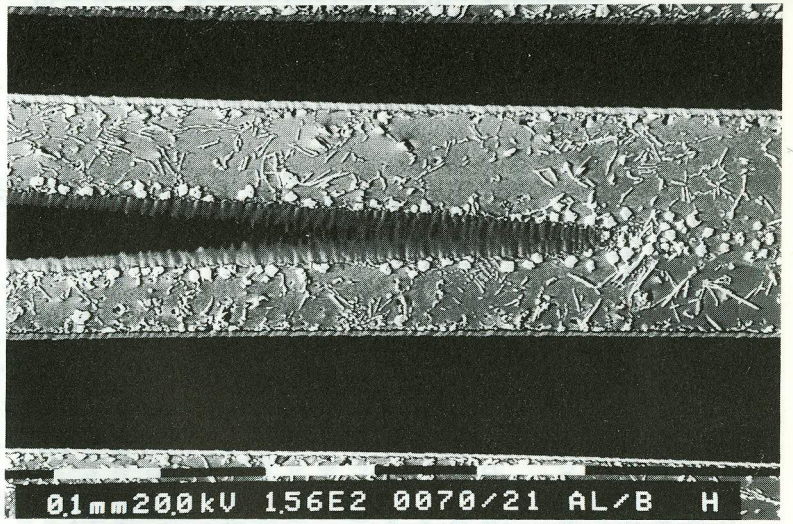


Fig. 2 Secondary electron image in the longitudinal direction of the 28% series material showing fibres, tapered fibre, matrix and second phases.

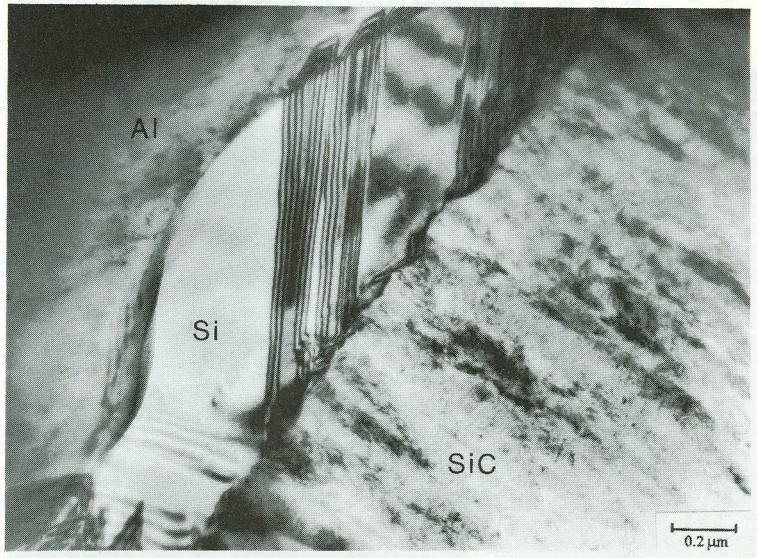


Fig. 4 Transmission electron micrograph showing the interface between the SiC coating and free silicon as twinned flake.

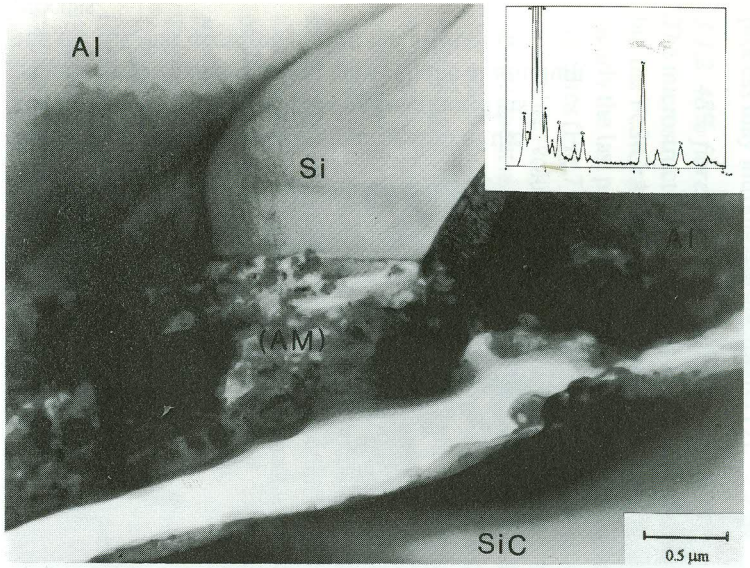


Fig. 5 Transmission electron micrograph of amorphous layer (AM) between SiC coating and aluminium alloy. Insert shows an energy dispersive spectrum from the layer.

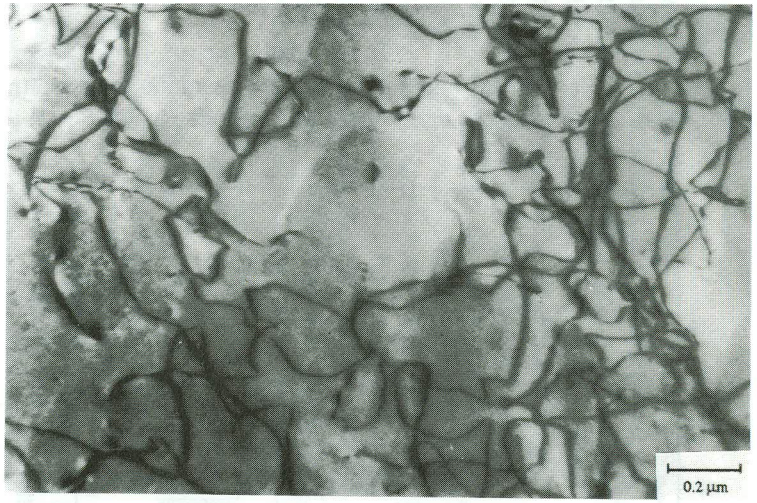


Fig. 6 Dislocation structure for the as received material 28% series B [001].

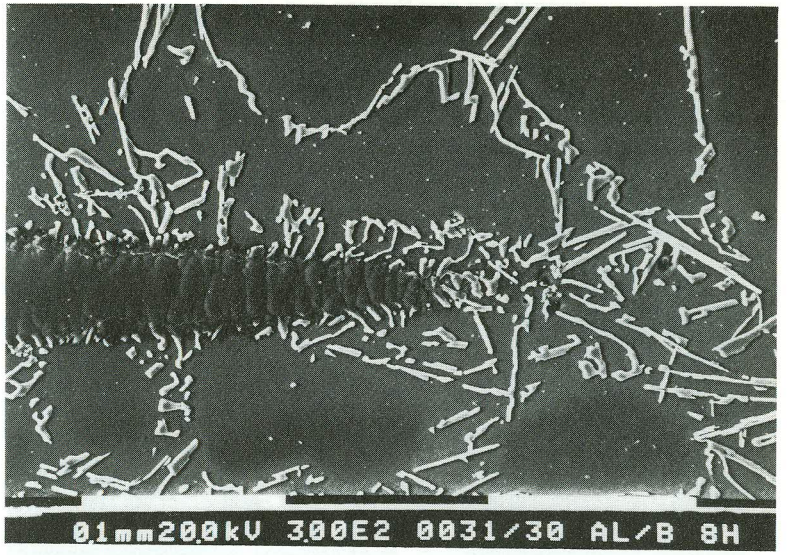


Fig. 7 Secondary electron image in the longitudinal direction of the 48% series material showing a tapered fibre and the matrix aluminium alloy.

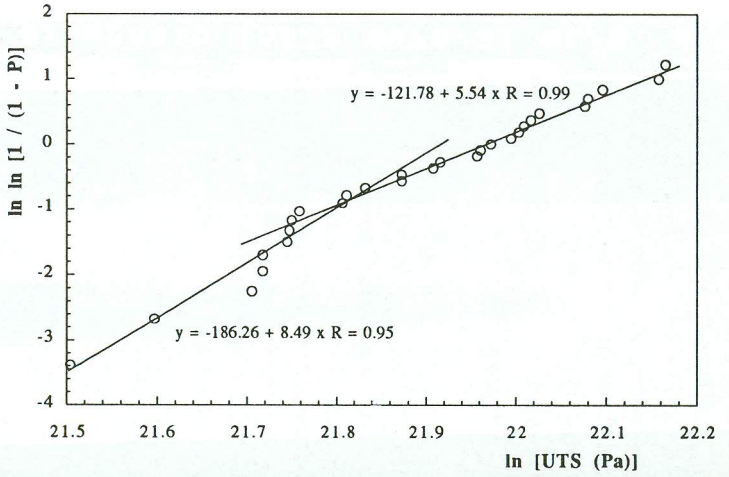


Fig. 8 Weibull plot of probability of failure against fibre strength showing two types of flaw distribution.

microstructural conditions.

The mean tensile strength of the fibres is the statistical result of many individual fibre tests and are best evaluated by the Weibull statistics [20]. Figure 8 shows a probability of failure plot against the fibre strength and it indicates a departure from linearity which may be due to a bimodal flaw distribution [21]. Similarly the work of Metcalfe [22] on boron fibres showed that this type of fibre contains populations of internal and surface flaws, each of which is characterized by a different distribution. Practically, these results indicate that the composite material will undoubtedly contain broken fibres after certain low stresses, below the average, have been applied.

*3.3 Fatigue testing*

The fatigue testing characterization, determined by plotting the number of elapsed cycles to failure versus maximum stress, suggests that the composite 28% series is only slightly sensitive to repeated tensile loading in the fibre direction, Fig.9. The large scatter in lifetime data is due to the complexity of damage development under cyclic loading and to large fabrication defects like slag inclusions, shrinkage porosity and transverse pieces of fibres. For the 48% series at 0° fibre orientation to the tensile axis, the fatigue tests show that the material has a stronger sensitivity to cyclic tensile loading (Fig.10). It was observed that both materials at 10° fibre orientation showed a significant decrease in fatigue strength, but the 48% series material revealed a higher decrease in fatigue strength. At this point it could be reasoned that the fatigue strengths of both materials are strongly dependent on microstructure and on the aluminium/fibre interface.

*3.4 Fatigue damage*

The fatigue damage, evaluated by plotting the fractional change in elastic modulus versus number of elapsed cycles, for the 28% series at 0° fibre orientation is shown in Fig. 11, for different stress ranges. At stress range $\Delta S$, ($\Delta S = S_{max} - S_{min}$), below 172 MPa it can be seen that this material shows a very small decreasing variation in the fractional change of secant modulus $\Delta E_S$. If the fatigue damage is translated into moduli variations, it can be suggested that under such conditions, the material is almost fatigue proof because very little damage is produced or detected. The stress-strain data under such circumstances shows that only closed hysteresis loops are generated. For a stress range around 214 MPa, the fatigue stress-strain behaviour changes. The first few cycles are characterized by open hysteresis loops that gradually close which usually represent a measure of work done in the material. Under this condition, after a few cycles, the fractional change of secant modulus increases while the matrix work hardens, till it attains a plateau and then starts decreasing due to fatigue damage. The initial increase in fractional modulus change depends 011 the stress range and would reach a maximum when it is equal to the ultimate tensile strength of the material. In this study the maximum increase in fractional secant modulus, for the 28% series, would be around 1.6% because one test has been made at $\sigma_{max} = 480$ MPa, which value is about the maximum range variation of the UTS of the material.

The above fatigue damage behaviour is also valid for the 48% series at 0° fibre orientation, but in this case, the material at stress range $\Delta S = 238$ MPa does not shows signs of stiffness loss but at stress range $\Delta S = 324$ MPa there is a clear change in the fractional secant modulus (Fig. 12).

A comparison between the shake down model and some experimental data shows that, if the shake down stress range is estimated by using equation (2), where $E_0$ is substituted by the average initial loading modulus, $E_m$ is the matrix modulus of elasticity and $\sigma_y^m$ is substituted by the matrix flow stress at a strain of 0.001, see Table 2, then $\Delta S_{sh} = 257$ MPa for the 28% series and a $\Delta S_{sh} = 341$ MPa for the 48% series. These average shake down stress ranges are higher than some experimental values, for instance one experiment for series 28% shows that at $\Delta S = 214$ MPa there is damage occurring in the material, the same is valid for series 48% at $\Delta S = 324$ MPa, vide Fig. 11 and Fig.12.

The shake down model has been applied successfully to some aluminium laminates reinforced with continuous fibres [1, 4, 23], the composites made by diffusion bonding. For these materials, the fatigue limits coincide with the composite shake down limits [1] or are reported to be lower then the composite's fatigue limit[4]. but the matrix flow stresses [8] or its cyclic flow strength[4] and fatigue limit seems to coincide. If not, the matrix stresses must be restricted to the level of the fatigue strength of the matrix in the composite material.

An attempt to evaluate the fatigue strength of the matrix aluminium alloy prior to infiltration was made under the same fatigue test conditions applied to the composite, Fig.13. The fatigue limit at $5 \times 10^6$ cycles was determined to be 64 MPa. Previous tests [4,23] for aluminium alloys in the annealed temper, have shown that the matrix fatigue limit coincides with the flow stress or the cyclic flow stress of the aluminium. The ratio of fatigue limit to tensile strength is about 0.5 and the ratio of fatigue limit to flow strength approaches unit [24]. The experimental results for the matrix prior to infiltration show such a correlation well, thus one would expect a fatigue limit of 54 MPa for the matrix under the infiltration condition, i.e. the same flow stress value, see Table 2. If this hypothetical fatigue limit is applied to the shake down model it will overestimate the shake down stress range. The shake down theory is based on the assumption that the fatigue resistance of the composite material is

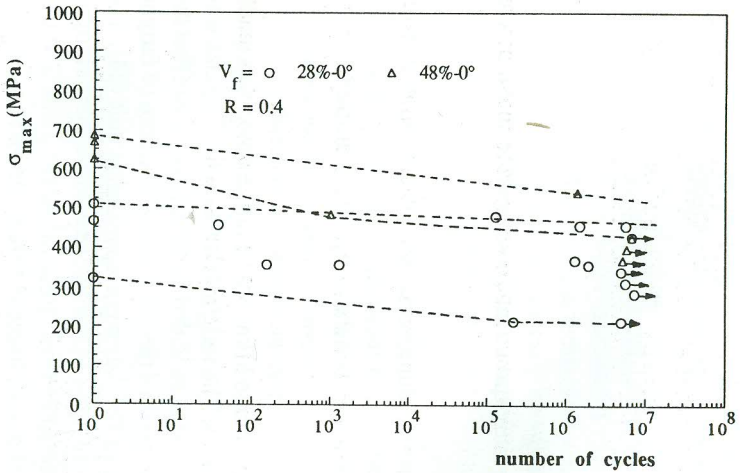


Fig. 9 S-N plot for the 28% and 48% series materials tested at 0° orientation.

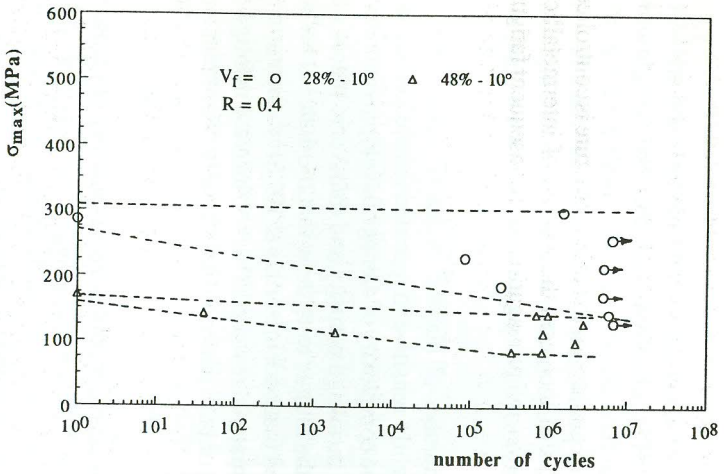


Fig. 10 S-N plot for the 28% and 48% series materials tested at 10° orientation.

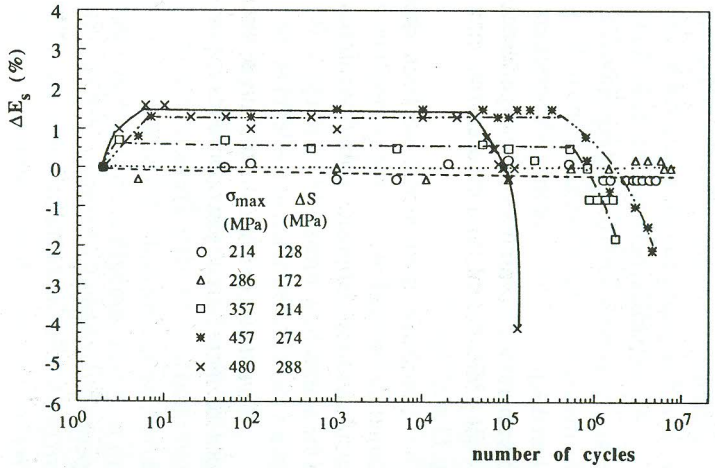


Fig. 11 Variation of the fractional change of elastic modulus versus number of cycles for the 28% series material tested at 0° orientation.

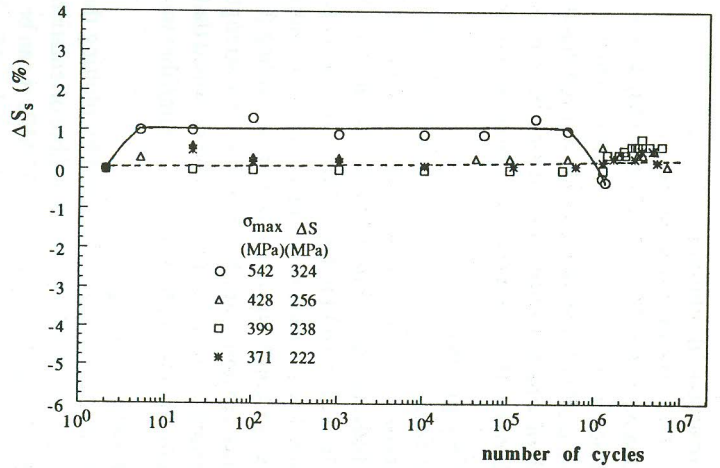


Fig.12 Variation of the fractional change of elastic modulus versus number of cycles for the 48% series material tested at 0° orientation.

determined by the fatigue strength of the constituents [1-4]. For composite materials produced by diffusion bonding, there is some control over the matrix microstructure if wrought alloys are used to produce the matrix. Thus, it is possible to relate the fatigue strength of the matrix alone with its fatigue strength in the composite material.

When the composite is made by a liquid metal infiltration technique, the matrix microstructure is controlled by the solidification kinetics together with contamination pick up that increases the amount of intermetallics present. These facts can affect the rate of fatigue microcrack nucleation and propagation, and consequent fatigue life. Thus, if it would be difficult to produce equivalent microstructures in the composite matrix and cast matrix alone, it would be difficult to correlate the composite matrix properties with the separated matrix.

*3.5 Microstructure characterization after mechanical testing*

Metallographic observations after fatigue testing show that there is cracking in the matrix of both 0° and 10° materials. The fibres are usually retained intact, bridging matrix fatigue cracks which are perpendicular to the tensile stress direction, Fig.14. It has been observed that fatigue cracks usually initiate at free surfaces, but they also can initiate inside the composite at fractured fibres, fibre ends and at fabrication defects. Circumstantial evidence also suggests that cracks may be initiated at intermetallic particles: such particles have negligible ductility and small microcracks are frequently observed to be associated with these particles. Depending on test stress range, these microcracks may appear early in life and their microscopic growth then takes place over the most portion of the fatigue lifetime. Because of many possible sites for crack initiation, and a non-uniform matrix/fibre interface, irregular fatigue fracture surfaces have been encountered Fig. 15.

The origin of the cracks at the free surface is associated with the stresses involved in the machining operation that can break fibres, crack silicon flakes embedded in the matrix or probably may crack intermetallics. The machining operation may not be the sole reason for surface particle cracking, the matrix plastic deformation during the fatigue test may induce cracks in the intermetallics or the silicon flakes [25]. Internally the material may contain cracked fibres that during the fatigue tests develop cracks; cracks also can evolve from fractured intermetallics or silicon flakes. Another internal source of cracks is shrinkage porosity and a Ti strip used to weave the fibres.

Crack growth, which can occur both transversely and longitudinally, is a consequence of different interfacial characteristics and fibre strength variation. For cyclic loading, when a crack front meets a weak fibre -matrix interface, crack branching may occur and the crack propagate along the matrix-fibre interface (Fig. 16). This will have a detrimental effect in the composite when it meets a weak fibre site causing its rupture. The material will eventually fail when the growth of fatigue cracks in the matrix impairs the load-bearing capacity of the composite.

Dislocation density measurements by TEM, on either tensile or fatigue tested specimens revealed no generate change when compared to the as received material (Fig.17). This means that the plastic deformation of the matrix material is inhomogeneous and should be highly concentrated around the fractured regions. The dislocation structure have been observed in regions around 5 mm away from the fracture surface and away from the matrix/fibre interface. In some areas the matrix shows many prismatic loops and dislocation debris (Fig.18).

## 4. Conclusions

The results of the present work suggest that fatigue damage of an aluminium alloy matrix composite, manufactured by a liquid metal infiltration technique, may be characterized by:

- the characteristics of the matrix microstructure and the fibre-matrix interface which affect the magnitude of the composite fatigue limit;
- a stiffness loss associated with fibre breakage and second phase cracked particles which lead to fatigue cracks in the matrix.

The results also show that the allowable composite stresses range in the shake down regime cannot be evaluated from the sole properties of the matrix and the fatigue behaviour is matrix dominated.

## 5. Acknowledgements

The authors acknowledge the support received from the Brazilian Government - CNPq/CNEN in the provision of a scholarship to J. L. R., and to the MOD for funding and material supply.

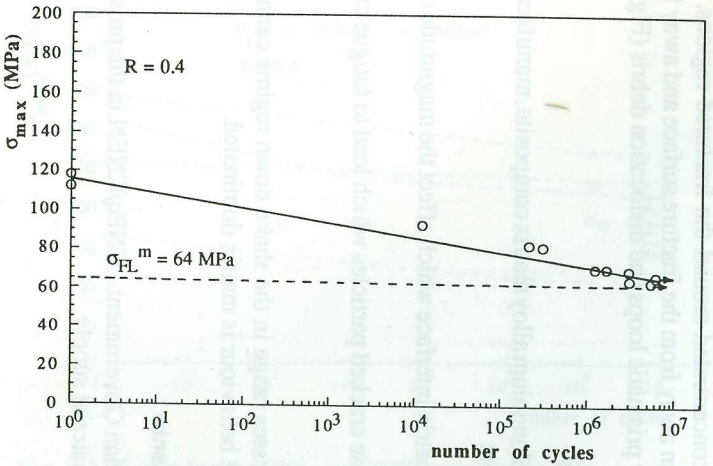


Fig. 13 Fatigue test results for the as cast aluminium alloy matrix prior to infiltration.

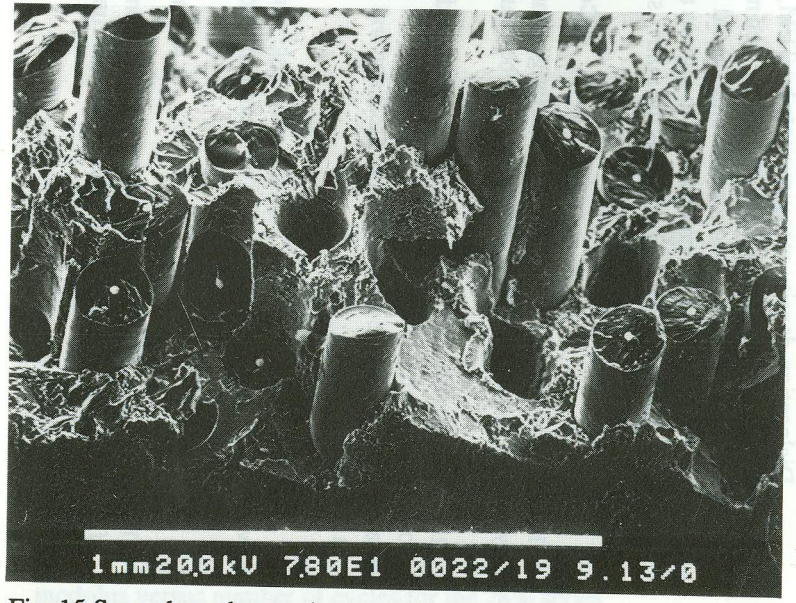


Fig. 15 Secondary electron image of fracture surface for the fatigued 48% series material.

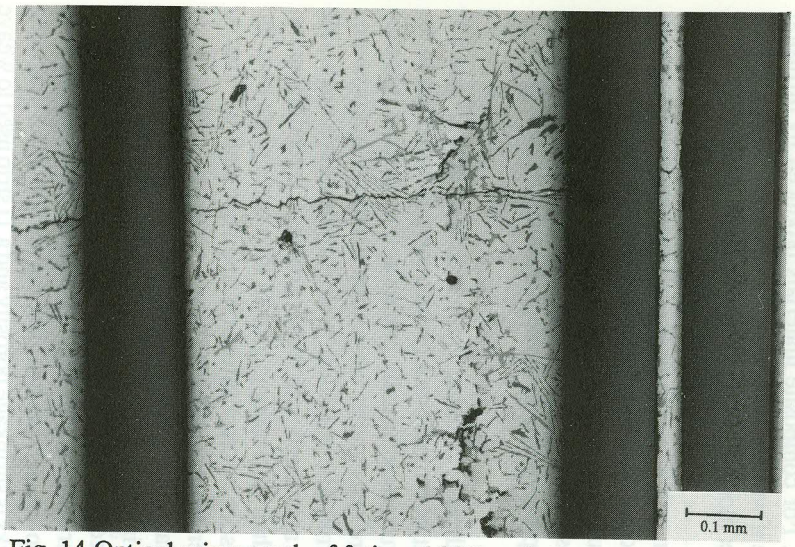


Fig. 14 Optical micrograph of fatigued 28% series material at $\Delta S$ = 288MPa, showing matrix cracks perpendicular to the stress direction and intact fibres.


Fig. 16 Secondary backscattered electron image of a surface origin crack and crack branching.

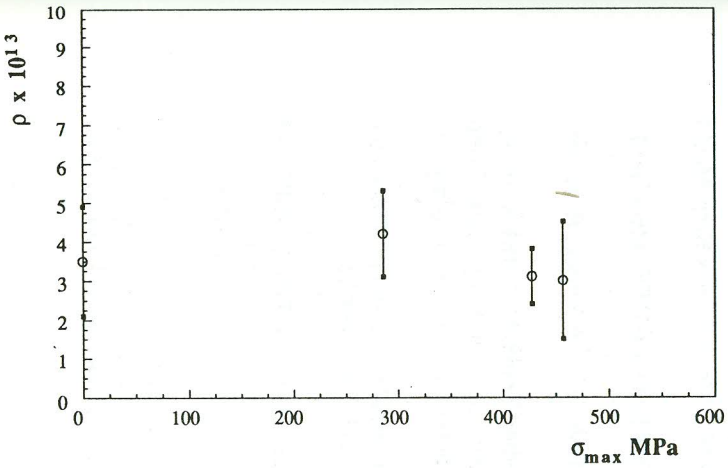


Fig. 17 Variation on dislocation densities in the aluminium alloy matrix with maximum stress for the 28% series material tested at 0° orientation.


Fig. 18 Dislocation structure showing prismatic loops and dislocation debris for the 28% series material B [112].

Table 1 Chemical compositions of aluminium alloys (wt%)

| | Si | Mg | Fe | Cu | Mn | Zn | Ti | - |
|---|---|---|---|---|---|---|---|---|
| ASM A356.0 | 6.5<br>7.5 | 0.25<br>0.45 | 0.20<br>max | 0.20<br>max | 0.10<br>max | 0.10<br>max | 0.20<br>max | b |
| present alloy prior to infiltration | 7.83 | 0.33 | 0.13 | - | 0.01 | 0.01 | 0.07 | - |

b - 0.05 max others (each); 0.15 others(total); rem. Al.

Table 2 Mechanical properties of fibre, matrix prior to infiltration, matrix infiltration condition and composite at different fibre orientations

| material properties | $V_f$ (%) | $Y_{0.1}$ (MPa) | UTS (MPa) | E (GPa) | $\varepsilon_p$(%) |
|---|---|---|---|---|---|
| fibre | - | - | 3235 | 383 | 0.84 * |
| aluminium alloy | - | 64±1 | 127±17 | 70 | 3.1±3.0 |
| matrix 28% | - | 54 | 116 | 69 | 1.5 |
| 28 - 0° | 29±2 | - | 379±91 | 164±9 | 0.11±0.07 |
| 28 - 10° | 30±2 | - | 281±7 | 158±11 | 0.23±0.09 |
| 28 - 90° | - | - | 36 | 100 | 0.01 |
| 48 - 0° | 47±2 | - | 661±37 | 218±6 | 0.05±0.02 |
| 48 - 10° | 46±1 | - | 171 | 205±11 | 0.5 |
| 48 - 90° | - | - | 26 | 134 | 0.01 |

(*) elastic deformation.

**References**

1.Dvorak, G. J. and Tar, J. Q. Fatigue and shakedown in metal matrix composites. In: Hancock, J. R., ch. Fatigue of Composite Materials. ASTM STP 569, 1975. 145-66.
2. Stinchcomb, W. W., Reifsnider, K. L., Marcus. L. A., Willians, R. S. Effects of frequency on the mechanical response of two composite materials. In: Hancock, J. R., ch. Fatigue of Composite Materials. ASTM STP 569, 1975. p. 116.
3. Dvorak, G. J. & Johnson, W. S. Fatigue damage mechanisms in boron - aluminium composite laminates. In: Bunsel, A. R., Bathias, C., Martrenchar, A., Menkes, D. Vercher, G., eds., Advances in Composite Materials v. 2, Pergamon, 1980. 1117 - 90.
4. Johnson, W. S. Modeling stiffness loss in boron/aluminum laminates below the fatigue limit. In: O'Brien, T. K., ed. Long Term Behaviour of Composites. ASTM STP 813, 1983. 160-78.
5. Charewicz, A. & Daniel, I. M. Damage mechanisms and accumulation in graphite/epoxy laminates. In: Hahn, H. T., ed. Composite Materials: Fatigue and Fracture. ASTM STP 907, 1984. p. 286.
(6) Toth, I. J. Creep and fatigue behavior of unidirectional and cross-plied composites. In: Composite Materials: Testing and Design. ASTM STP 460, 1969. 236-53.
(7) Mikura, N. Metal matrix composites - present applications and future potential. In: The Institute of Metals. Abstracts conf. on.... London. 23rd - 24th Nov., 1987.
(8) Melan, E. Der Spannungszustand eines "Hencky-Mises'schen" Kontinuums bei veraenderlicher Belastung. Sitz. Ak. Wiss. Wien, 147:73-87, 1938. Apud Johnson, W. S. Fatigue damage accumulation in various metal matrix composites. National Aeronautics and Space Administration, NASA Tech. Memo 89116, Mar., 1987.
9. Symonds, P. S. Shakedown in continuous media. J. Appl. Mech., Mar., 1951. 85-9.
10. Trumper, R. L., Sherwood, P. J., Clifford, A. W. Metal matrix composites. In: The Royal Aeronautical Society, Material in Aerospace. Proc. conf. on..., London 2nd - 4th April . v. 2, 1986. p. 250.
11. American Society for Metals. Properties and selection of nonferrous alloys and pure metals. In: Metals Handbook. 9th Ed., v. 2,1989. p. 167.
12. Morley, J. G. High-Performance Fibre Composites Academic, 1987. p. 40.
13. Stuhrke, W. F. The mechanical behavior of aluminum-boron composite material. In: Herzog, J. A., ch. Metal Matrix Composites. ASTM STP 438,1968. p. 121.
14. Mondolfo, L. F. Aluminium Alloys: Structure and Properties. London, Butterworth, 1976. p. 534.
15. Rivlin, V. G. & Raynor, G. V. Critical evaluation of constitution of aluminium-iron-silicon system. Int. Met. Rev., 3: 133-152,1981.
16. Ping Liu & Dunlop G. L. Long-range ordering of vacancies in bcc α-AlFeSi. J. Mat Sci. 23: 1419-24, 1988.
17. Fu, L. -J., Schmerling, M., Marcus, H. L. Interfaces studies of aluminum metal matrix composites. In: Hahn, H. T., ed. Composite Materials: Fatigue and Fracture. ASTM STP 907, 1986. p. 63.
18. Arsenault, R. J. & Fisher, R. M. Microstructure of fiber and particulate SiC in 6061 Al composites. Scrp. Metall. 17: 67-71,1983.
19. Hancock, J. R. & Grosskreutz, J. C. Plastic yielding and strain distribution in filament-reinforced metals. In: Herzog, J. A., ch. Metal Matrix Composites. ASTM STP 438, 1968. 134-49.
20. Corten, H. T. Micromechanics and fracture behavior of composites. In: Brout, L. J. & Knock, R. H., eds. Modern Composite Materials. Addison-Wesley, 1967. p. 49.
21. Hughes, J. D. H., A review of techniques for evaluating stiff fibres. Br. Ceram. Trans. J. 87: 181-8, 1988.
22. Metcalfe, A. G., Influence of interaction on fracture of metal matrix-filament composites. Monsanto Symp. on ... Oct. 1967. Apud Tetelman, A. S. Fracture processes in fiber composite materials. In: Composite Materials; Testing and Design ASTM STP 460, 1969. 473-502.
23. Johnson, W. S. & Wallis, R. R. Fatigue behavior of continuous fiber silicon carbide / aluminum composites. In: HAHN, H. T., ed. Composite Materials: Fatigue and Fracture. ASTM STP 907, 1986. 161-75.
24. Van Horn, K. R. Aluminum. v. 1, ASM 1967. p. 183.
25. Gangulee, A. & Gurland, J. On the fracture of silicon particles in aluminum-silicon alloys. Trans. AIME, 239: 269-72,1967.